



## Effect of TiO<sub>2</sub> content on the crystallization and the color of (ZrO<sub>2</sub>,TiO<sub>2</sub>)-doped Li<sub>2</sub>O–Al<sub>2</sub>O<sub>3</sub>–SiO<sub>2</sub> glasses

M. Chavoutier<sup>a</sup>, D. Caurant<sup>a,\*</sup>, O. Majérus<sup>a</sup>, R. Boulesteix<sup>a</sup>, P. Loiseau<sup>a</sup>, C. Jousseume<sup>b</sup>, E. Brunet<sup>b</sup>, E. Lecomte<sup>c</sup>

<sup>a</sup> Laboratoire de Chimie de la Matière Condensée de Paris (UMR CNRS 7574), Chimie-ParisTech, 11 rue Pierre et Marie Curie, 75005 Paris, France

<sup>b</sup> Saint-Gobain Recherche, 39 quai Lucien Lefranc, 93303 Aubervilliers, France

<sup>c</sup> Eurokera, 1 bis avenue du Général-de-Gaulle, Chierry, 02400 Château-Thierry, France

### ARTICLE INFO

#### Article history:

Received 27 December 2012

Received in revised form 25 March 2013

Available online 24 April 2013

#### Keywords:

Crystallization;

LAS glass–ceramics;

Coloration;

Li<sub>2</sub>O–Al<sub>2</sub>O<sub>3</sub>–SiO<sub>2</sub> glasses;

XANES

### ABSTRACT

Glass–ceramics formed by controlled crystallization of Li<sub>2</sub>O–Al<sub>2</sub>O<sub>3</sub>–SiO<sub>2</sub> (LAS) parent glasses are well-known for their low thermal expansion and transparency. In order to promote bulk crystallization, it is necessary to add nucleating agents like TiO<sub>2</sub> and ZrO<sub>2</sub> to the glass composition leading to ZrTiO<sub>4</sub> nuclei during heating, followed by the crystallization of a β-quartz phase that transforms into β-spodumene at higher temperature. Generally, these glass–ceramics present a yellowish-brown coloration whose intensity increases with the crystallization rate and that is partly due to coloring elements like titanium. In this study, we investigated the origin of the evolution of the color of LAS glasses and glass–ceramics by varying the TiO<sub>2</sub> concentration. To do this, several TiO<sub>2</sub>-bearing LAS glasses (with TiO<sub>2</sub> ranging from 0 to 4 mol% and 1 mol% ZrO<sub>2</sub>) were prepared and heat treated at a given temperature (925 °C) to study the impact of the TiO<sub>2</sub> concentration on their crystallization behavior and their color. The crystallization and microstructure of LAS glasses and glass–ceramics were studied by DTA, XRD and TEM whereas their structure was investigated by EPR, optical and X-ray absorption spectroscopies. From all the results obtained, the evolution of the optical absorption and coloration of LAS glasses and glass–ceramics was mainly explained by Ti<sup>4+</sup>–O<sup>2-</sup> charge transfer (glasses) and by gap absorption and Rayleigh scattering of nanocrystals (glass–ceramics).

© 2013 Elsevier B.V. All rights reserved.

### 1. Introduction

Glass–ceramics can be defined as composite materials that are formed by controlled crystallization of glasses (parent-glasses) in their bulk. The most well-known transparent glass–ceramics are based on the Li<sub>2</sub>O–Al<sub>2</sub>O<sub>3</sub>–SiO<sub>2</sub> (LAS) system and are used in cook top panels for kitchen stoves and in fireplace glass doors because of their heat resistance and low thermal expansion (<10<sup>-6</sup> K<sup>-1</sup>) [1,2]. In order to induce homogeneous crystallization in their bulk, it is necessary to add small amounts of nucleating agents like TiO<sub>2</sub> and ZrO<sub>2</sub> to the glass composition [1]. It is well known that the ratio Ti:Zr = 2:1 in mol% is the most efficient [3] but this result is not fully understood. According to recent results [4–6], the crystallization starts with the liquid–liquid phase separation of (ZrO<sub>2</sub>, TiO<sub>2</sub>, Al<sub>2</sub>O<sub>3</sub>)-rich droplets that then fully crystallize as ZrTiO<sub>4</sub> nanocrystals whereas an Al<sub>2</sub>O<sub>3</sub>-enriched glassy layer (diffusion barrier) forms around these nanocrystals hampering their growth and ripening. This nucleation stage is followed by the crystallization of a metastable β-quartz phase close to LiAlSi<sub>2</sub>O<sub>6</sub> composition as major phase that then transforms into stable β-spodumene at higher temperature [1,7]. It has been recently proposed that the β-quartz phase does not

nucleate directly on the surface of the ZrTiO<sub>4</sub> nanocrystals by an epitaxial mechanism, but rather in their close surrounding where the composition of the supercooled melt is more favorable because of the existence of a sharp composition gradient [4,6].

The (TiO<sub>2</sub>, ZrO<sub>2</sub>)-doped LAS parent glasses have generally a yellowish-brown color. Their coloration may be due to the presence of transition metals leading to absorption in the near UV and visible range. The transition metal elements present in LAS parent glasses are Ti and Zr as nucleating agents and Fe as impurity. ZrO<sub>2</sub> is not known to give any color to the glass. Indeed, the Zr<sup>4+</sup> ion has a 4d<sup>0</sup> electronic configuration (lack of d–d transition) and the O–Zr charge transfer band (CTB) probably occurs at wavelengths lower than 200 nm [8]. The Ti<sup>3+</sup> cation with 3d<sup>1</sup> electronic configuration has a d–d absorption close to 500 nm [9,10]. Besides, the Ti<sup>4+</sup> cation with its 3d<sup>0</sup> electronic configuration does not give rise to d–d absorption but it can contribute to optical absorption of the glass in the near UV due to O–Ti charge transfer. The position of the corresponding CTB varies according to the relative positions of the glass valence band (mainly composed of oxygen 2p orbitals) and the Ti<sup>4+</sup> 3d orbitals. In silicate glasses, depending on their composition, Ti<sup>4+</sup> cations can be 4-, 5- and/or 6-fold coordinated which may thus influence the position of the CTB. The presence of iron as impurity (Fe<sup>2+</sup> (3d<sup>6</sup>), Fe<sup>3+</sup> (3d<sup>5</sup>)) in raw materials also contributes to the parent glasses absorption in the UV and visible range (O–Fe charge transfer and d–d

\* Corresponding author. Tel.: +33 1 53737922; fax: +33 1 46347489.

E-mail address: [daniel-caurant@chimie-paristech.fr](mailto:daniel-caurant@chimie-paristech.fr) (D. Caurant).

transitions) [11,12]. Moreover, the possibility of intervalence charge transfer between  $\text{Fe}^{2+}$  and  $\text{Ti}^{4+}$  cations may also contribute to glass coloration if these cations are close enough in glass structure [13].

The glass–ceramic color is more pronounced and more brownish after crystallization [14]. The origin of the darker coloration of LAS glass–ceramics in comparison with parent glasses may be linked to both structural and microstructural evolutions inducing for instance changes in the position of the d–d absorption and charge transfer bands and to light scattering by the small crystals formed inside the glass [3].

In this study, we have studied the origin of the color of ( $\text{ZrO}_2$ ,  $\text{TiO}_2$ )-doped LAS glasses and its evolution after partial crystallization ( $\text{ZrTiO}_4$  and  $\beta$ -quartz) by varying the  $\text{TiO}_2$  concentration from 0 to 4 mol%, while keeping constant the  $\text{ZrO}_2$  concentration (1 mol%). The evolution of the color of the LAS glasses and glass–ceramics with  $\text{TiO}_2$  content has been followed by optical transmission and diffuse reflectance, whereas the glass crystallization, the nature and the distribution of the crystalline phases have been investigated respectively by differential thermal analysis (DTA), X-ray diffraction (XRD) and transmission electron microscopy (TEM). The evolution of the environment (coordination) of  $\text{Ti}^{4+}$  and  $\text{Zr}^{4+}$  cations in LAS glasses and glass–ceramics has been probed by X-ray absorption near edge structure (XANES) spectroscopy also using glassy and crystalline reference samples containing  $\text{Ti}^{4+}$  or  $\text{Zr}^{4+}$  cations in known coordination state. After crystallization, a particular emphasis was put on the incorporation of  $\text{Ti}^{4+}$  and  $\text{Zr}^{4+}$  cations in the  $\text{ZrTiO}_4$  phase and on its impact on the coloration of the glass–ceramics. The occurrence of  $\text{Fe}^{3+}$  (impurity of raw materials) and  $\text{Ti}^{3+}$  cations – that may also affect the coloration of LAS glasses and glass–ceramics – was checked by electron paramagnetic resonance (EPR). From all the results obtained, the origin of the evolution of the coloration of LAS glasses and glass–ceramics with  $\text{TiO}_2$  concentration and crystallization is discussed by considerations on charge transfer and d–d transitions implying titanium and gap absorption and scattering of nanocrystals.

## 2. Experimental

### 2.1. Glasses and glass–ceramics preparation

The composition of the LAS parent glasses with increasing  $\text{TiO}_2$  contents (referred to as LAS-x glasses where x represents the  $\text{TiO}_2$  content in mol% from 0 to 4 mol%) prepared for this study is given in Table 1. Appropriate amounts of reagent grade  $\text{SiO}_2$ ,  $\text{Li}_2\text{CO}_3$ ,  $\text{Al}_2\text{O}_3$ ,  $\text{ZrO}_2$  and  $\text{TiO}_2$  powders were mixed and melted in Pt crucibles during 6 h at 1650 °C, in air atmosphere. After a first quench of the melt to room temperature, glasses were grounded and melted again at 1650 °C during 4 h to increase the melt homogeneity before quenching. In order to avoid nucleation risks that could affect their properties (such as optical absorption), the glass samples were not annealed after quenching. All the quenched samples were transparent and amorphous according to XRD measurements. A comprehensive analysis of the glass LAS-3 was performed by Induced Coupled Plasma (ICP) at the SCA Solaize (France) and showed that its composition was very close to the nominal composition (Table 1). For all other glasses only the  $\text{TiO}_2$  content was analyzed by ICP and analyzed and nominal concentrations were also very close.

**Table 1**  
Nominal composition (mol%) of LAS-x glasses. x represents the  $\text{TiO}_2$  content in mol%.

Glass	LAS-0	LAS-1	LAS-2	LAS-3	LAS-4
$\text{SiO}_2$	74.50	73.80	73.00	72.20 (71.70) <sup>a</sup>	71.50
$\text{Al}_2\text{O}_3$	13.30	13.10	13.00	12.90 (13.19) <sup>a</sup>	12.70
$\text{Li}_2\text{O}$	11.20	11.10	11.00	10.90 (11.01) <sup>a</sup>	10.80
$\text{ZrO}_2$	1.00	1.00	1.00	1.00 (1.09) <sup>a</sup>	1.00
$\text{TiO}_2$	0.00	1.00	2.00	3.00 (3.01) <sup>a</sup>	4.00

<sup>a</sup> Concentrations determined by ICP analysis for LAS-3 glass.

The concentration of  $\text{Fe}_2\text{O}_3$  from raw materials was determined by ICP analysis only for two glass samples of the LAS-x series (LAS-2 (270 ppm), LAS-3 (415 ppm) in wt.%). At these levels, it appeared that the impact of iron on the coloration of LAS glass could be neglected (see below Fig. 4).

For the glass–ceramics preparation (referred to as LASGC-x glass–ceramics), all LAS-x parent glasses (bulk samples) were heat treated following the same thermal treatment consisting in a heating ramp at 5 °C/min from room temperature to 925 °C, then a 12 min dwell at 925 °C and a controlled cooling to room temperature at 50 °C/min in the furnace. These thermal treatment conditions were chosen to obtain transparent glass–ceramic samples. As it will be shown below, the value of the temperature chosen in this study (925 °C) enables to form  $\beta$ -quartz for the LAS-x samples with  $\text{TiO}_2$  concentration higher than or equal to 1 mol% (Fig. 1).

To serve as references for X-ray absorption experiments and/or optical absorption, several crystalline and glassy samples were used. Stoichiometric  $\text{ZrTiO}_4$  powder was synthesized from pure  $\text{TiO}_2$  and  $\text{ZrO}_2$  powders by solid-state reaction at 1450 °C during 3 h. The single phase character of this reference sample was verified by XRD. Crystalline commercial compounds ( $\text{ZrO}_2$  (baddeleyite),  $\text{ZrSiO}_4$  (zircon),  $\text{TiO}_2$  (rutile)) and glasses ( $\text{Ba}_2\text{TiSi}_2\text{O}_8$ ,  $\text{K}_2\text{TiSi}_4\text{O}_{11}$  and a Zr-doped peralkaline sodium aluminosilicate  $\text{Na}_{3.42}\text{AlSi}_{6.96}\text{Zr}_{0.01}\text{O}_{17.27}$ ) were selected as Ti and Zr X-ray absorption references [15,16].  $\text{K}_2\text{TiSi}_4\text{O}_{11}$  glass was prepared by mixing appropriate amounts of reagent grade  $\text{SiO}_2$ ,  $\text{K}_2\text{CO}_3$  and  $\text{TiO}_2$  powders followed by melting during 6 h at 1400 °C in air and then quenching to room temperature. Similarly, appropriate amounts of reagent grade  $\text{SiO}_2$ ,  $\text{Na}_2\text{CO}_3$ ,  $\text{Al}_2\text{O}_3$  and  $\text{ZrO}_2$  powders were mixed for the preparation of the Zr-doped sodium aluminosilicate glass and then melted in air during 6 h at 1400 °C and 2 h at 1500 °C. After a first quench of the melt to room temperature, the glass was grounded and melted again at 1500 °C during 3 h 30 min to increase the melt homogeneity before another quenching.

### 2.2. Glasses and glass–ceramics characterization

All LAS-x glasses were studied by DTA with a Netzsch STA 409 apparatus. Approximately 200 mg of crushed glass samples (particle size between 80 and 125  $\mu\text{m}$ ) was heated in Pt crucibles from room temperature to 1450 °C at 5 °C/min in the DTA apparatus ( $\text{Al}_2\text{O}_3$  powder was used as a reference material). The glass transformation temperature  $T_g$  was determined from DTA curves (slight endothermic effect at low temperature, Table 2). The exothermic peaks were all associated with crystallization phenomena and were attributed with the help of XRD (Table 2). For this, LAS-x powder glass samples of similar particle size were heated at

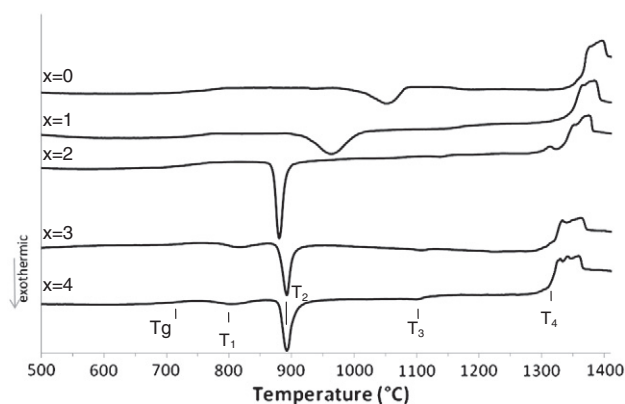


**Fig. 1.** DTA curves of LAS-x glasses. The temperatures associated with glass transformation  $T_g$  and crystallization phenomena ( $T_1$  ( $\text{ZrTiO}_4$ ),  $T_2$  ( $\beta$ -quartz),  $T_3$  ( $\beta$ -spodumene)) are reported in Table 2. The endothermic event observed above  $T_4$  is associated with the melting of the crystalline phases formed during the DTA run.

the same rate (5 °C/min) to the temperature of the peak and were then quenched to room temperature before XRD characterization.

All LAS-x glass and LASGC-x glass–ceramic samples were characterized by XRD with the help of a PANalytical X'Pert Pro diffractometer using Cu-K $\alpha$  radiation ( $\lambda = 0.15406$  nm) to check the existence and the nature of crystalline phases.

Several samples (LASGC-2, LASGC-3, LASGC-4) were also studied by Transmission Electron Microscopy (TEM). Samples for TEM investigations were prepared from crushed LASGC-x pieces deposited on a carbon coated 300 mesh copper grid. The bright field images were recorded with a 2k ultrascan 1000 Gatan camera (2048  $\times$  2048 pixels), using a LaB<sub>6</sub> JEOL JEM2100 microscope operating at 200 kV.

All glass and glass–ceramic samples were cut and polished ( $\approx 2.5$  mm thickness) before recording their optical transmission spectra (200–800 nm) at room temperature with a Cary 6000i spectrophotometer. The colorimetric coordinates  $L^*$ ,  $a^*$  and  $b^*$  have been determined for all the glasses and glass–ceramics in the CIE 1976 color space using the optical transmission spectra and the CIE standard illuminant A (Table 4). In order to limit the saturation observed on transmission spectra due to the strong absorption in the UV and near UV range, diffuse reflectance spectra (R) were also recorded from crushed samples (particle size <50  $\mu$ m) placed in powder cell with the same Cary 6000i spectrophotometer by using a diffuse reflectance accessory consisting of a 110 mm diameter integrating sphere with a PTFE coating. A PTFE sample was also used as reference. All diffuse reflectance spectra were then processed using the Kubelka–Munk transformation  $F(R)$  according to Eq. (1) that enables to compare the spectra obtained by diffuse reflectance to those obtained by transmission:

$$F(R) = (1 - R^2) / 2R \quad (1)$$

where R is the reflectance of the sample (%). To facilitate the study of the impact of TiO<sub>2</sub> content on the optical absorption of our glasses, the contribution of the matrix (gap absorption) was removed from diffuse reflectance spectra by subtracting – after the Kubelka–Munk transformation – the spectrum of the glass without TiO<sub>2</sub> (LAS-0 sample) to all LAS-x samples ( $x > 0$ ). They were then simulated as the sum of Gaussian contributions to extract the absorption bands and study their evolution with composition changes.

The occurrence of Ti<sup>3+</sup> (3d<sup>1</sup>) and Fe<sup>3+</sup> (3d<sup>5</sup>) paramagnetic cations in glasses and glass–ceramics was checked by EPR. Spectra were recorded at X band (9.5 GHz) at 30 K with the help of Bruker ELEXYS E500 spectrometer.

The evolution of the local environment of Ti and Zr in both glasses and glass–ceramics was followed by recording Ti and Zr K-edge XANES spectra. These spectra were recorded at room temperature in fluorescence mode for the Ti K-edge and in transmission mode for the Zr K-edge at the Advance Photon Source of the Argonne National Laboratory (IL, USA), beam line 20-BM, using a Si(111) double crystal monochromator. The model compounds used for the study of Ti K-edge spectra were Ba<sub>2</sub>TiSi<sub>2</sub>O<sub>8</sub> and K<sub>2</sub>TiSi<sub>4</sub>O<sub>11</sub> glasses (with Ti in 5-fold coordination [16]), TiO<sub>2</sub> rutile and ZrTiO<sub>4</sub> crystalline powders (with Ti in 6-fold

coordination) (Table 3). The model compounds used for the study of the Zr K-edge spectra were the Zr-doped sodium aluminosilicate glass and ZrTiO<sub>4</sub> for the Zr 6-fold coordination, ZrO<sub>2</sub> baddeleyite (with Zr in 7-fold coordination) and ZrSiO<sub>4</sub> zircon (with Zr in 8-fold coordination). The X-ray absorption spectra of all our samples were normalized and compared to those of the model compounds to determine the Ti and Zr coordination (Table 3).

### 3. Results

#### 3.1. Differential thermal analysis study of parent glasses

The DTA curves of LAS-x glasses are shown in Fig. 1. The characteristic temperatures of glass transformation  $T_g$  and crystallization (ZrTiO<sub>4</sub>,  $\beta$ -quartz and  $\beta$ -spodumene) are given in Table 2. In accordance with the fluidifying effect of TiO<sub>2</sub> on glass melts [17], a decrease of  $T_g$  is observed with increasing TiO<sub>2</sub> content at least for the highest titanium concentrations. Moreover, a significant evolution of the width at half maximum and peak temperature ( $T_2$ ) of the exothermic effect associated with  $\beta$ -quartz crystallization is observed when TiO<sub>2</sub> concentration increases. For low TiO<sub>2</sub> concentrations (0–1 mol%), the  $\beta$ -quartz crystallization peak remains broad but shifts to lower temperature when TiO<sub>2</sub> is introduced in glass composition (1 mol%). This exothermic effect for these concentrations is mainly associated with  $\beta$ -quartz crystallization, but other crystalline phases are observed like  $\beta$ -spodumene and ZrO<sub>2</sub> or ZrTiO<sub>4</sub>. When increasing TiO<sub>2</sub> concentration (2 mol%), the  $\beta$ -quartz crystallization peak shifts to lower temperature and an important decrease of its width is observed. For higher TiO<sub>2</sub> concentrations (3–4 mol%), the  $\beta$ -quartz crystallization peak does not significantly change whereas a new crystallization peak is detected at a lower temperature  $T_1$ . The crystallization associated with the  $T_1$  temperature is not easy to attribute as the XRD pattern consists in a single broad weak peak around 30.5°. The attribution will be discussed in the following part. All these results – and more particularly the evolution of the DTA peak width – indicate that for low TiO<sub>2</sub> concentrations (0–1 mol%) the  $\beta$ -quartz crystallization mainly occurs from glass surface whereas for higher TiO<sub>2</sub> concentrations (2–4 mol%)  $\beta$ -quartz mainly crystallizes directly in the bulk (thin DTA exothermic peak displaced towards low temperature). For more details about the relation between DTA curves and crystallization mechanisms (bulk/surface) see for instance [18]. These DTA curves confirm the choice of 1 mol% ZrO<sub>2</sub>/2 mol% TiO<sub>2</sub> as the most efficient ratio to obtain significant nucleation in the bulk. Indeed more TiO<sub>2</sub> does not imply any changes in the  $\beta$ -quartz crystallization peak. Besides, these DTA curves allow also choosing the heat treatment temperature to obtain transparent glass–ceramics.

#### 3.2. X-ray diffraction study of glass–ceramics

After heat-treatment, each LASGC-x sample was characterized by XRD. The XRD patterns of LASGC-x samples with  $x = 2, 3$  and 4 all exhibit the diffraction peaks associated with the  $\beta$ -quartz phase (JCPDS

**Table 2**

Characteristic temperatures (°C) of LAS-x glasses determined from DTA curves (Fig. 1), with  $T_g$  glass transformation temperature,  $T_1$  temperature of ZrTiO<sub>4</sub> crystallization,  $T_2$  temperature of  $\beta$ -quartz crystallization and  $T_3$  temperature of  $\beta$ -spodumene crystallization. ZrTiO<sub>4</sub> crystallization was not detected by DTA for LAS-0, LAS-1 and LAS-2 samples. Uncertainties on the measurement of T values are given in parenthesis.

Glass	$T_g$	$T_1$	$T_2$	$T_3$
LAS-0	700 (10)	–	1051 (3)	1183 (10)
LAS-1	710 (10)	–	963 (2)	1150 (10)
LAS-2	700 (10)	–	880 (1)	1135 (5)
LAS-3	690 (10)	810 (5)	892 (1)	1105 (5)
LAS-4	670 (10)	795 (5)	892 (1)	1097 (5)

**Table 3**

Position in eV and normalized height of the pre-peak of XANES spectra (Ti K-edge) of model compounds (Ba<sub>2</sub>TiO<sub>4</sub> [25], Ba<sub>2</sub>TiSi<sub>2</sub>O<sub>8</sub>, K<sub>2</sub>TiSi<sub>4</sub>O<sub>11</sub>, TiO<sub>2</sub> (rutile), ZrTiO<sub>4</sub>) and LAS-x glasses.

	CN	Position (eV)	Normalized height
Ba <sub>2</sub> TiO <sub>4</sub>	4	4969.4	1.00
Ba <sub>2</sub> TiSi <sub>2</sub> O <sub>8</sub>	5	4970.6	0.67
K <sub>2</sub> TiSi <sub>4</sub> O <sub>11</sub>	5	4970.7 $\pm$ 0.3	0.48
r-TiO <sub>2</sub>	6	4971.6 $\pm$ 0.3	0.31
ZrTiO <sub>4</sub>	6	4970.7 $\pm$ 0.3	0.21
LAS-1	–	4970.0 $\pm$ 0.3	0.66
LAS-2	–	4970.0 $\pm$ 0.3	0.65
LAS-3	–	4970.0 $\pm$ 0.3	0.63
LAS-4	–	4970.0 $\pm$ 0.3	0.59

file N°00-040-0073) and a broad diffraction peak around  $30.5^\circ$  that can be attributed to  $\text{ZrTiO}_4$  crystals as it is usually done (Fig. 2). However, as this has already been reported [4], the attribution of the peak around  $30.5^\circ$  is not easy. Indeed, this peak is a single wide and weak peak (Fig. 2), and other phases such as tetragonal or cubic zirconia, brookite or  $\text{Zr}_{1-x}\text{Ti}_x\text{O}_4$  with  $x \neq 0$  are also known to exhibit XRD peaks in the same angular range. Nevertheless, this peak is usually attributed to  $\text{ZrTiO}_4$  due to the glass composition.

In accordance with the DTA curves (Fig. 1), no spodumene was detected on the XRD patterns of all the LASGC-x samples because they were all heated at  $925^\circ\text{C}$  (i.e. at a temperature lower than  $T_3$ ). LASGC-0 and LASGC-1 samples only exhibit a broad peak characteristic of a totally amorphous material due to the absence of crystallization below  $925^\circ\text{C}$  for these samples ( $T_2 > 925^\circ\text{C}$ ). LASGC-0 and LASGC-1 samples that are not crystallized will not be studied further in this paper.

### 3.3. Transmission electron microscopy study of glasses and glass-ceramics

The amorphous and homogenous microstructure of LAS-x glasses was checked by TEM (Fig. 3a). After heat-treatment,  $\text{ZrTiO}_4$  nanocrystals were detected by TEM in the samples [4,19] (Fig. 3b–d). LASGC-2, LASGC-3 and LASGC-4 samples present different concentrations of crystals with different morphologies. Droplet-shape crystals of about 5 nm diameter were encountered in all these three samples. However, the LASGC-2 sample presents in addition  $5 \times 15$  nm rods in small quantity (Fig. 3b). In LASGC-3 and LASGC-4 samples, the density of spherical crystals is higher than in LASGC-2 and no rods can be observed.  $\beta$ -quartz crystals that exist in LASGC-2, 3 and 4 samples according to XRD (Fig. 2) are difficult to observe by TEM as these crystals become amorphous under the electron beam.

### 3.4. Optical absorption study of glasses and glass-ceramics

#### 3.4.1. Optical absorption of glasses

Before dealing with the impact of adding increasing  $\text{TiO}_2$  amounts on the optical absorption and thus on the coloration of LAS glasses and glass-ceramics, it was interesting to consider if the presence of iron coming from raw materials had or had no significant impact on their coloration. According to the ICP analyses,  $\text{Fe}_2\text{O}_3$  was present at rather low concentration in the glasses of the LAS-x series (lower than 420 ppm, expressed as  $\text{Fe}_2\text{O}_3$  in wt.%). In this case, Fig. 4 showed that the presence of  $\text{Fe}_2\text{O}_3$  had only a low impact on their optical absorption in the visible range (400–750 nm) and on their coloration. Indeed, by preparing glasses with 2 mol%  $\text{TiO}_2$  and with  $\text{Fe}_2\text{O}_3$  concentration ranging from 315 to 1345 ppm (in wt.%), it was shown that the effect of  $\text{Fe}_2\text{O}_3$  became significant only for LAS glasses with  $\text{Fe}_2\text{O}_3$  concentration higher than 600–700 ppm: an increasing optical absorption was detected in the

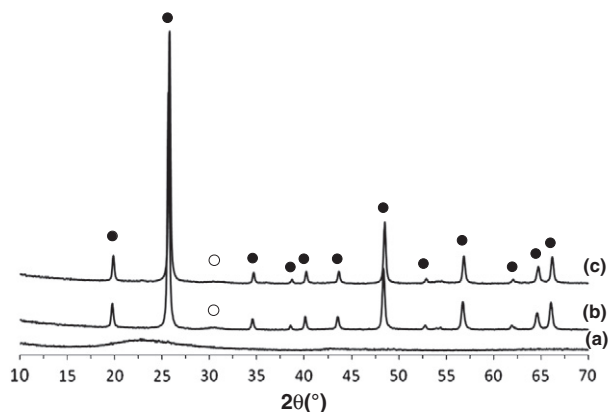


Fig. 2. XRD patterns of LASGC-0 (a), LASGC-2 (b) and LASGC-4 (c) samples heat treated at  $925^\circ\text{C}$ . (•:  $\beta$ -quartz (JCPDS file 00-040-0073), ○:  $\text{ZrTiO}_4$  (JCPDS file 34-0415)).

UV-blue and in the IR-red ranges associated with a shift of the coloration towards yellow (Fig. 4) due to  $\text{Fe}^{3+}$  and  $\text{Fe}^{2+}$  cation absorption, with a possible contribution of an intervalence charge transfer between  $\text{Fe}^{2+}$  and  $\text{Ti}^{4+}$  cations.

The optical transmission and diffuse reflectance spectra of all LAS-x glasses are presented in Fig. 5. The pictures of the samples and the evolution of the corresponding colorimetric  $a^*$  and  $b^*$  coordinates are also shown in Fig. 5 and in Table 4. A shift of the absorption gap towards higher wavelengths was observed on the transmission spectra with increasing  $\text{TiO}_2$  concentration that is responsible for the evolution of the coloration from almost uncolored (LAS-0 and LAS-1 glasses) to increasingly yellow-brown (LAS-2, LAS-3, LAS-4 glasses) (Fig. 5a). Diffuse reflectance enables to avoid saturation in the UV and near UV ranges and shows that the increase of  $\text{TiO}_2$  concentration has a strong impact on the spectra. Indeed, UV absorption increases and progressively shifts towards lower energy (Fig. 5b). It can be noted that no absorption band around 500 nm – that could be associated with  $\text{Ti}^{3+}$  cations – is detected either on the transmission or the diffuse reflectance spectra. This is in agreement with the pale color of all LAS-x samples ( $\text{Ti}^{3+}$ -bearing compounds are darker) and is coherent with what is known for silicate glasses containing  $\text{Ti}^{3+}$  cations [10,20]. After the Kubelka–Munk transformation, the diffuse reflectance spectra  $f(R)$  of LAS-x glasses can be deconvoluted with the help of 2 or 3 Gaussian bands depending on glass composition (Fig. 6). Whereas only 2 Gaussian contributions (at 4.9 eV and 6.1 eV) are needed to simulate the spectra of LAS-1 and LAS-2 samples (Fig. 6a), it is necessary to use a supplementary Gaussian contribution at lower energy (4.4 eV) when the  $\text{TiO}_2$  concentration is higher than 2 mol% (Fig. 6b). Even if the exact origin of these Gaussian bands is not known with certainty, they are mainly due to charge transfer transitions from the 2p orbitals of oxygen anions to the 3d orbitals of  $\text{Ti}^{4+}$  cations. Due to the crystal field created by the oxygen anions surrounding the  $\text{Ti}^{4+}$  cations in the glass, their 3d orbitals are split into two main groups which cause the two main bands observed on the spectra of Fig. 6a. An evolution of the average  $\text{Ti}^{4+}$  cations environment – and thus of the crystal field in their surrounding – with  $\text{TiO}_2$  concentration could explain the new bands observed for the highest  $\text{TiO}_2$  concentrations (Fig. 6b).

#### 3.4.2. Optical absorption of glass-ceramics

The transmission spectra of LASGC-0 and LASGC-1 samples are very similar to those of the corresponding parent glasses (spectra not shown) which is in accordance with the fact that these samples are not crystallized (see Section 3.2). On the contrary, the LASGC-2, LASGC-3 and LASGC-4 samples exhibit darker coloration (Fig. 7b and Table 4) than the corresponding parent glasses (Fig. 5a and Table 4). In the spectra (Fig. 7a), this evolution of coloration is materialized by a shift of the optical gap towards higher wavelengths and a decrease of transmission in the 400–600 nm range. This decrease of transmission in the visible range can be linked to light scattering by nanocrystals. Indeed, since Rayleigh scattering is proportional to  $1/\lambda^4$  ( $\lambda$  being the light wavelength), the transmission was plotted versus  $1/\lambda^4$  and the resulting curve found out to be linear in the 400–600 nm part (inset in Fig. 7). Moreover, the shape of the optical gap evolves with  $\text{TiO}_2$  concentration and becomes straighter as the  $\text{TiO}_2$  concentration increases. Diffuse reflectance spectra were also recorded for all glass-ceramics, LAS-2 glass and  $\text{TiO}_2$  (rutile) and  $\text{ZrTiO}_4$  reference powders (Fig. 8). A strong evolution of absorption is observed between the glass and the glass-ceramics, indeed a strong shift of the gap towards the visible range is observed. The glass-ceramics show a strong absorption band that can be attributed to the  $\text{ZrTiO}_4$  gap absorption for LASGC-x samples. LASGC-3 and LASGC-4 samples present in addition a shoulder around 3.8 eV that could be related to  $\text{TiO}_2$  absorption. Noticeably, no absorption is detected in the 400–600 nm range (i.e. below 3.1 eV) of these diffuse reflectance spectra, confirming the fact that the transmission decrease in this range (Fig. 7) was due to Rayleigh light scattering.

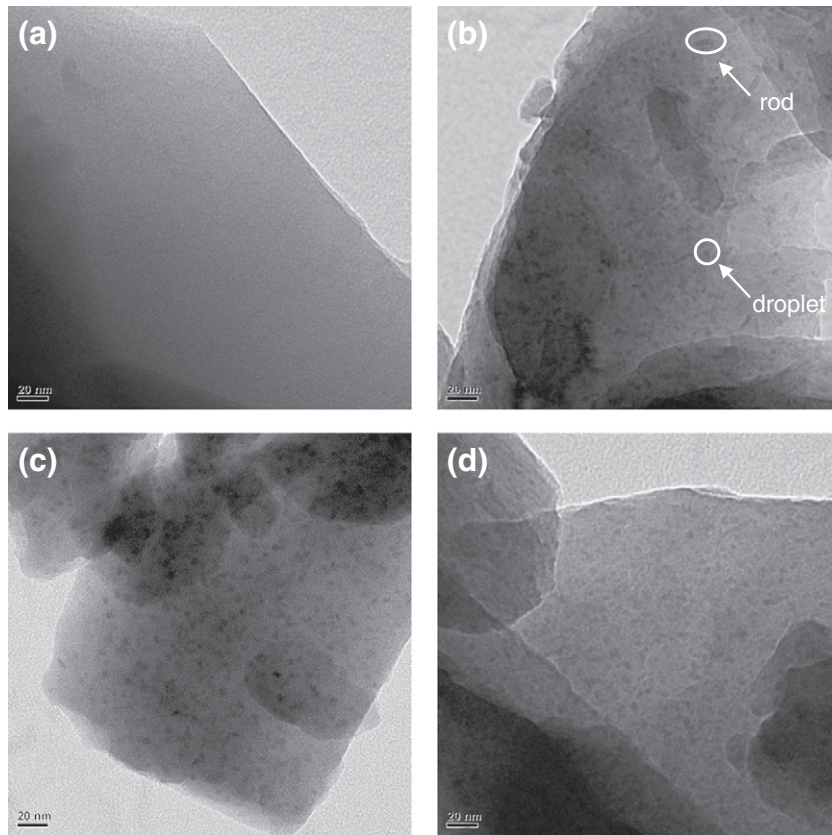


**Fig. 3.** TEM images of LAS-2 (a), LASGC-2 (b), LASGC-3 (c) and LASGC-4 (d) samples. Examples of nano-sized  $\text{ZrTiO}_4$  particles of different shapes are shown in (b).

### 3.5. Electron paramagnetic study of glasses and glass-ceramics

The EPR spectra of LAS-x glasses are shown in Fig. 9. By comparison with a Ti-rich reference calcium aluminosilicate glass sample (spectrum not shown) containing  $\text{Ti}^{3+}$  cations associated with a characteristic sharp EPR signal at a g factor close to 1.9 (i.e. at a magnetic field close to 3500 G), it clearly appears that no  $\text{Ti}^{3+}$  cations are present in our samples whatever the  $\text{TiO}_2$  concentration. However, it is interesting to note that the intensity of the EPR signal at  $g = 4.3$  (i.e. at a magnetic

field close to 1580 G) associated with  $\text{Fe}^{3+}$  cations in low symmetry sites [21,22] – present as impurities in our glasses – decreases as the  $\text{TiO}_2$  concentration increases. This shows that the amount of  $\text{Fe}^{3+}$  cations in LAS-x glasses decreases with  $\text{TiO}_2$  addition and suggests that  $\text{TiO}_2$  has a reducing effect on the  $\text{Fe}^{3+}/\text{Fe}^{2+}$  redox couple by promoting the formation of  $\text{Fe}^{2+}$  cations that are not detected by EPR ( $\text{Fe}^{2+}$  is a non-Kramers ion). To explain this evolution, we propose that a small amount of  $\text{Ti}^{3+}$  cations is formed in the melt at high temperature (displacement towards the right of the endothermic

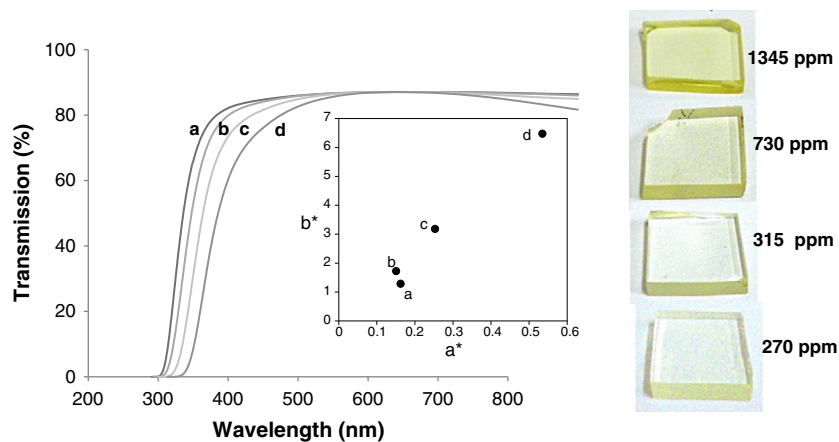


**Fig. 4.** Evolution of the optical transmission spectra of LAS glasses of composition similar to that of the LAS-2 glass given in Table 1 (2 mol%  $\text{TiO}_2$ ) with various  $\text{Fe}_2\text{O}_3$  concentrations (a: 270 ppm (glass LAS-2), b: 315 ppm, c: 730 ppm, d: 1345 ppm as analyzed by ICP in  $\text{Fe}_2\text{O}_3$  wt.%). The pictures of the LAS-x glass samples – that are presented on the right of the figure with their  $\text{Fe}_2\text{O}_3$  contents – show an increase of the intensity of the yellowish color when  $\text{Fe}_2\text{O}_3$  concentration increases. The corresponding evolution of coloration ( $a^*$  and  $b^*$  colorimetric coordinates in the CIE 1976 ( $L^*$ ,  $a^*$ ,  $b^*$ ) color space) of glasses with increasing  $\text{Fe}_2\text{O}_3$  concentration is also shown (inset). For all glasses presented in this figure with  $\text{Fe}_2\text{O}_3$  concentration higher than 270 ppm (wt%), iron oxide was added intentionally to glass composition before melting, this was not the case for the LAS-x glass series studied in this paper.

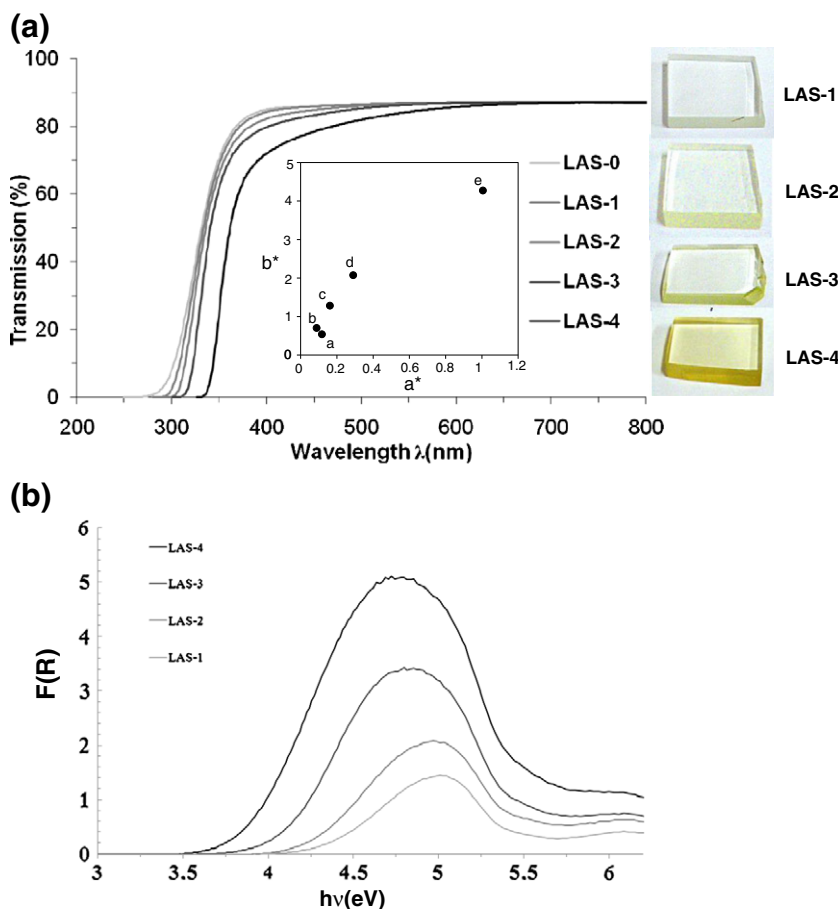


**Fig. 5.** (a) Transmission and (b) diffuse reflectance (after Kubelka–Munk transformation  $F(R)$  and subtraction of the spectrum of the glass without  $\text{TiO}_2$  (LAS-0 sample)) spectra of LAS- $x$  glasses. The pictures of the LAS- $x$  glass samples ( $x = 1$  to 4) that are presented in (a) show an increase of the intensity of the yellowish-brown color when  $\text{TiO}_2$  concentration increases (the LAS-1 glass is almost colorless). The corresponding evolution of the  $a^*$  and  $b^*$  colorimetric coordinates in the CIE 1976 ( $L^*$ ,  $a^*$ ,  $b^*$ ) color space of LAS- $x$  glasses is also shown in the inset of (a) ((a) LAS-0, (b) LAS-1, (c) LAS-2, (d) LAS-3, (e) LAS-4).

$\text{Ti}^{4+} \leftrightarrow \text{Ti}^{3+}$  redox equilibrium with temperature) that then reacts quantitatively with  $\text{Fe}^{3+}$  cations to form  $\text{Fe}^{2+}$  cations according to the following redox equilibrium:  $\text{Ti}^{3+} + \text{Fe}^{3+} \leftrightarrow \text{Ti}^{4+} + \text{Fe}^{2+}$ . Indeed, it is well known that  $\text{Ti}^{3+}$  has a high reducing power on the  $\text{Fe}^{3+}/\text{Fe}^{2+}$  redox couple according to different redox couple classifications reported in literature for silicate glasses [23,24]. Thus, the decrease of the intensity of the EPR signal associated with  $\text{Fe}^{3+}$  cations could be explained by a shift towards the right of the previous redox equilibrium when the  $\text{TiO}_2$  concentration increases.

In the case of LASGC- $x$  glass-ceramic samples, their EPR spectra still do not show any  $\text{Ti}^{3+}$  cations (spectra not shown). Consequently,

the darker color of glass-ceramics is not due to the formation of  $\text{Ti}^{3+}$  cations during thermal treatment.

### 3.6. X-ray absorption study of glasses and glass-ceramics

#### 3.6.1. X-ray absorption study of glasses

The environment of Ti and Zr in LAS- $x$  glasses was studied by XANES (Fig. 10). It is interesting to point out that the XANES spectra at Ti K-edge remain almost identical whatever the  $\text{TiO}_2$  concentration, indicating that  $\text{Ti}^{4+}$  ions have the same average environment for this  $\text{TiO}_2$  concentration range in the LAS- $x$  glass. The pre-edge position is  $4970.0 \pm 0.3$  eV and the pre-edge intensity is around 0.65 for all LAS- $x$  glasses. Table 3 gives the pre-edge position and intensity ranges for Ti in four, five and six-fold coordinations in model compounds, as reported in [25] and as measured in this work. By comparing the results of LAS- $x$  glasses with that of our references and with that of the model compounds published in literature [25], the LAS- $x$  Ti-K pre-edges are more intense than that in five-fold coordinated Ti-compounds (Fig. 10a) and are located at a higher energy than that of the four-fold coordinated Ti-compounds ( $4970.0 \pm 0.3$  eV compared with 4969.4 eV reported for Ti in  $\text{Ba}_2\text{TiO}_4$  [25]). Although these differences are at the resolution limit of these spectra, both features indicate that titanium is present in a mixture of fourfold and fivefold coordination environment in the LAS- $x$  glasses. It is difficult to determine the percentage of  $\text{Ti}^{4+}$  four- and five-fold coordinated as the couple of pre-edge data (position, intensity) belongs to a common field for these two coordinations. However, the X-ray absorption results obtained by Höche et al. [5] for similar LAS glass at the Ti-L3 edge indicate

**Table 4**

Colorimetric coordinates  $L^*$ ,  $a^*$  and  $b^*$  of LAS- $x$  glasses and LASGC- $x$  glass-ceramics in the CIE 1976 color space using the optical transmission spectra (Figs. 5 and 7) and the CIE standard illuminant A [27]. When  $a^*$  increases the coloration becomes more red whereas it becomes more yellow when  $b^*$  increases according to the  $L^*a^*b^*$  color space. Uncertainties:  $L^* (\pm 0.20)$ ,  $a^* (\pm 0.15)$ ,  $b^* (\pm 0.15)$ .

Sample	$L^*$	$a^*$	$b^*$
LAS-1	94.66	0.11	0.52
LAS-2	96.01	0.08	0.64
LAS-3	94.71	0.10	1.10
LAS-4	95.80	0.25	1.74
LASGC-0	94.80	1.08	4.55
LASGC-2	93.89	0.09	0.50
LASGC-3	92.24	0.64	4.09
LASGC-4	93.67	0.76	4.19

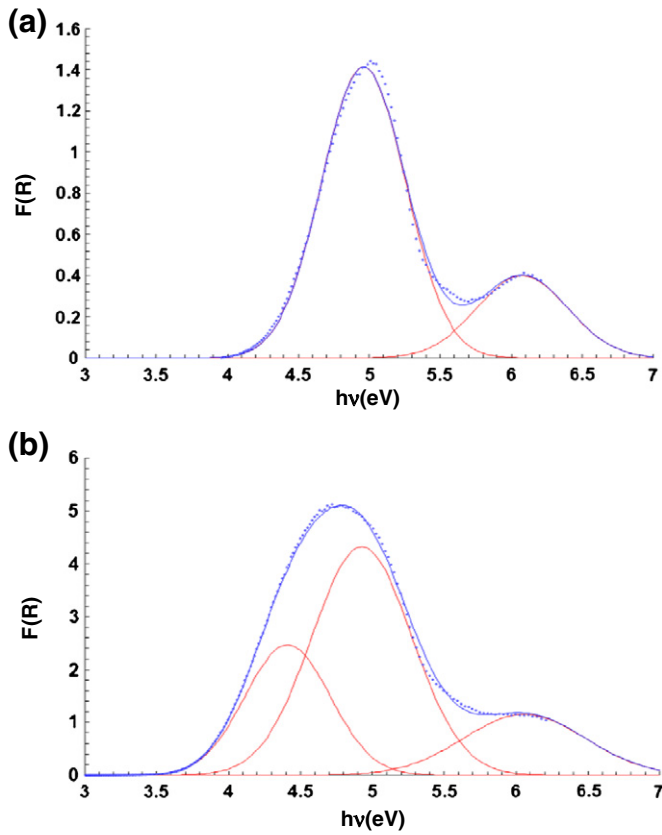


**Fig. 6.** Examples of deconvolution of the Kubelka–Munk transformed diffuse reflectance spectra of LAS-0 (a) and LAS-4 (b) glasses with the help of two or three Gaussian bands. Solid line (simulated spectrum and Gaussian components). Dotted line (experimental spectrum).

that  $\text{Ti}^{4+}$  cations are more likely fivefold coordinated. These results suggest that in our LAS-x glass samples, the percentage of  $\text{Ti}^{4+}$  in fivefold coordination is high (more than 50%).

XANES spectra at the Zr K-edge do not display sharp features so that the determination of the coordination of Zr in LAS-x glasses is more complex. Considering the XANES spectra of the glassy or crystalline model compounds, some peaks are present for several coordination states but some of them are characteristic of one kind of coordination (Fig. 10b): a shoulder (A) at 18,003 eV for seven-fold coordinated Zr species, a late peak (E) at 18,050 eV together with a peak (B) at 18,016 eV for eight-fold coordinated Zr species and a high intensity peak (D) at 18,028 eV for six-fold coordinated Zr species. The Zr K-edge XANES spectrum of  $\text{ZrTiO}_4$  presents the shoulder (A) in addition to a high intensity peak (D). According to the  $\text{ZrTiO}_4$  structure determined by XRD, the average (Ti, Zr) site is an octahedron distorted along a binary axis, with two additional oxygens lying as second neighbors within 3 Å of the (Ti, Zr) center. It is possible that the Zr site is locally distinct from this average environment and close to a seven-fold coordination, which could account for the (A) and (D) spectral features. The Zr K-edge spectra of LAS-x glasses are close to that of  $\text{ZrTiO}_4$  with feature (D) having a higher intensity. This suggests either a distorted  $\text{ZrO}_6$  environment close to that in  $\text{ZrTiO}_4$ , or a mixture of  $\text{ZrTiO}_4$ -type sites and more regular 6-fold coordination sites, for  $\text{Zr}^{4+}$  ions in these glasses.

### 3.6.2. X-ray absorption study of glass-ceramics

Some more information on the Ti and Zr environments after the crystallization process can be obtained by XANES measurements. Fig. 11 shows the Ti K-edge XANES spectra before and after heat-treatment of the LAS-2 sample. They are compared with the spectrum of the  $\text{ZrTiO}_4$  powder at Ti K-edge.

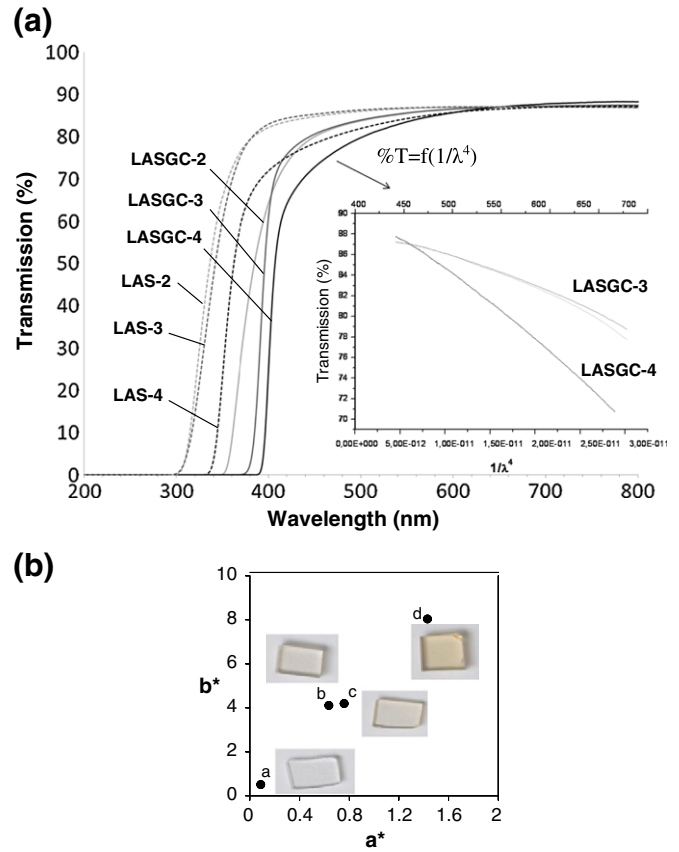


**Fig. 7.** (a) Transmission spectra of LAS-x (in dotted line) and LASGC-x (in straight line) samples. In the inset, the transmission is plotted versus  $1/\lambda^4$  in the range 400–700 nm for LASGC-3 and LASGC-4 samples. (b) Evolution of the  $a^*$  and  $b^*$  colorimetric coordinates in the CIE 1976 ( $L^*$ ,  $a^*$ ,  $b^*$ ) color space of the LASGC-x glass-ceramics ((a) LASGC-0, (b) LASGC-2, (c) LASGC-3, (d) LASGC-4). The pictures of the samples are also shown in the figure.

After heat-treatment, an intensity decrease and a shift towards higher energy of the pre-peak are observed at the Ti K-edge (Fig. 11a). These changes in the XANES spectra indicate that the average Ti coordination in the glass-ceramic increases. Moreover, as shown in Fig. 11a the XANES spectrum of the LASGC-2 glass-ceramics can be remarkably well simulated (dotted line) by a linear combination of the XANES spectra of  $\text{ZrTiO}_4$  and LAS-2 glass, with 46% of  $\text{ZrTiO}_4$  contribution. This last value is coherent with the initial ratio  $\text{Ti}:\text{Zr} = 2:1$  in mol% in the parent LAS-2 glass where the  $\text{ZrO}_2$  content is the limiting factor for  $\text{ZrTiO}_4$  crystallization, and suggests that the

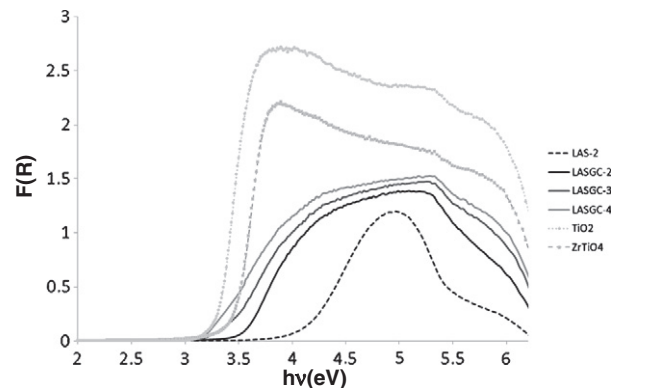


**Fig. 8.** Diffuse reflectance spectra (after Kubelka–Munk transformation) of LAS-2 glass, LASGC-2, LASGC-3, LASGC-4 glass-ceramics,  $\text{ZrTiO}_4$  and  $\text{TiO}_2$  (rutile) powders.

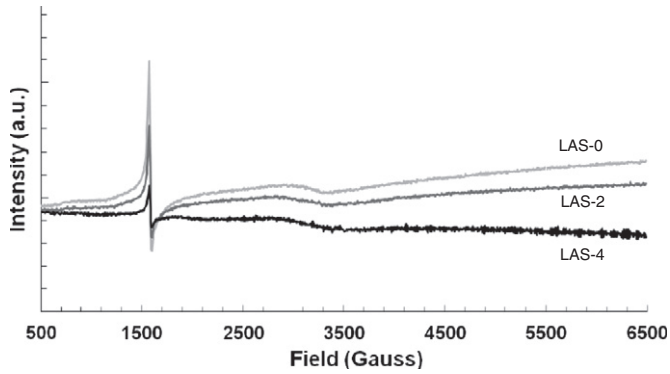


**Fig. 9.** EPR spectra of LAS-*x* glasses (X-band, *T* = 30 K). The sharp signal at *g* ~ 4.3 (1580 G) and the broad and weak signal at *g* ~ 2.0 (3500 G) are due to Fe<sup>3+</sup> paramagnetic impurities from raw materials.

ZrTiO<sub>4</sub> crystals have a composition close to stoichiometry. Note that the reported maximum value *x* for the Zr<sub>1-x</sub>Ti<sub>1+x</sub>O<sub>4</sub> solid solution at room temperature is 0.34, so that all the Ti<sup>4+</sup> ions initially present in the parent glass may potentially be inserted in Zr<sub>1-x</sub>Ti<sub>1+x</sub>O<sub>4</sub> solid solution crystals [26], but only half of all Ti present was finally inserted in ZrTiO<sub>4</sub> crystals. At last, the adequacy of this simulation also indicates

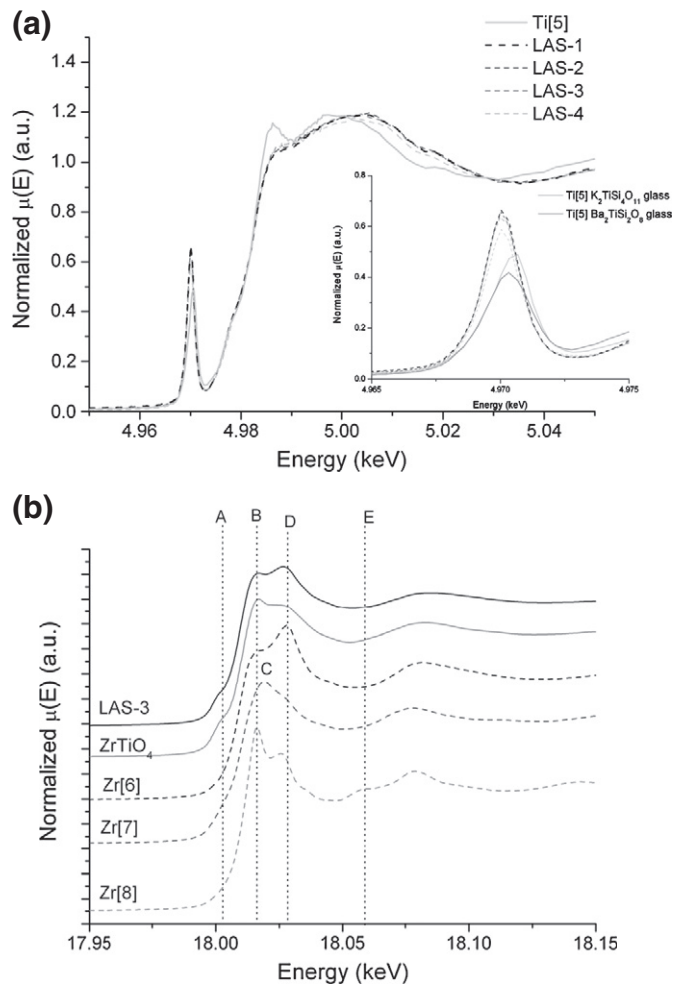


**Fig. 10.** (a) XANES spectra at Ti K-edge of LAS-*x* glasses and of two reference glass samples with Ti in five-fold coordination (K<sub>2</sub>TiSi<sub>4</sub>O<sub>11</sub> and Ba<sub>2</sub>TiSi<sub>2</sub>O<sub>8</sub>). The inset shows a zoom of the pre-edge region around 497 eV. (b) XANES spectra at Zr K-edge of LAS-3 glass, ZrTiO<sub>4</sub> and model compounds with Zr in 6-fold (Zr-doped sodium aluminosilicate glass [15] and ZrTiO<sub>4</sub>), in 7-fold (ZrO<sub>2</sub> (baddeleyite)) and in 8-fold (ZrSiO<sub>4</sub>) coordination.

that the Ti<sup>4+</sup> ions, which are not inserted in the ZrTiO<sub>4</sub> crystals, keep a local environment close to that in the parent glass (mixture of 4- and 5-coordination states).

The evolution of the XANES spectra at Ti K-edge as a function of TiO<sub>2</sub> concentration in the LASGC-*x* glass-ceramics is shown in Fig. 12. From 2 to 4 mol% TiO<sub>2</sub> content, the Ti K-edge pre-peak intensity decreases and a second pre-peak appears at 4.974 keV that is a characteristic of the 6-fold coordination. By considering all their features, the Ti K-edge XANES spectra are consistent with a greater fraction of Ti<sup>4+</sup> cations in a 6-fold coordination environment when the TiO<sub>2</sub> content increases. Notably in the LASGC-4 sample, the Ti K-edge crest is very similar to that of the rutile r-TiO<sub>2</sub> phase (note the sharp peak at 5.004 keV in Fig. 12a, that is common to r-TiO<sub>2</sub>), while the pre-edge features more closely match that of ZrTiO<sub>4</sub>. A linear combination of XANES spectra with 81% contribution of ZrTiO<sub>4</sub> and 19% of LAS-4 reproduces the experimental spectrum at the pre-edge (but not at the crest), while no convenient combination can be found with r-TiO<sub>2</sub>. Considering that during X-ray absorption processes, the absorbing electron stays on the coordination polyhedron at the pre-edge energy, while it leaves the polyhedron with a mean free path of 10–15 Å at the edge-crest energy, the spectrum of the LASGC-4 sample suggests that a great majority of Ti<sup>4+</sup> cations are incorporated in r-TiO<sub>2</sub> type crystals with local distortion of the octahedron as in ZrTiO<sub>4</sub>. The thermodynamic domain of Zr<sub>1-x</sub>Ti<sub>1+x</sub>O<sub>4</sub> solid solution extends up to Zr<sub>0.66</sub>Ti<sub>1.34</sub>O<sub>4</sub> [19], but the

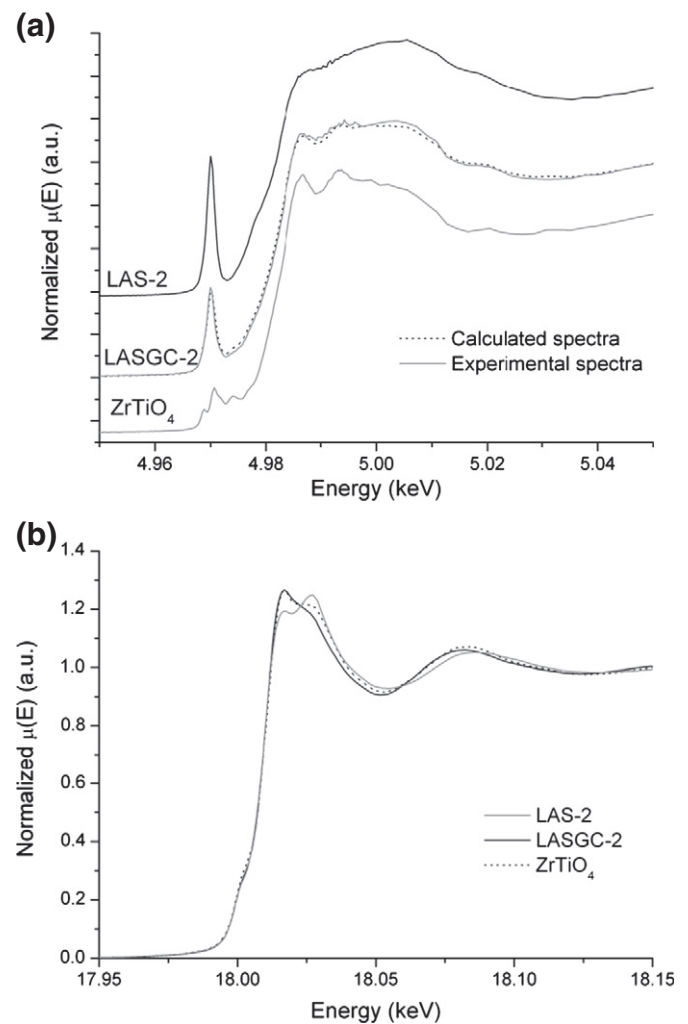


**Fig. 11.** (a) XANES spectra at Ti K-edge of LAS-2, LASGC-2 and ZrTiO<sub>4</sub> samples (straight line) and spectra calculated as a linear combination of the XANES spectra of ZrTiO<sub>4</sub> and LAS-2 glass with 46% of ZrTiO<sub>4</sub> (dotted line). (b) XANES spectra at Zr K-edge of LAS-2, LASGC-2 and ZrTiO<sub>4</sub> samples.

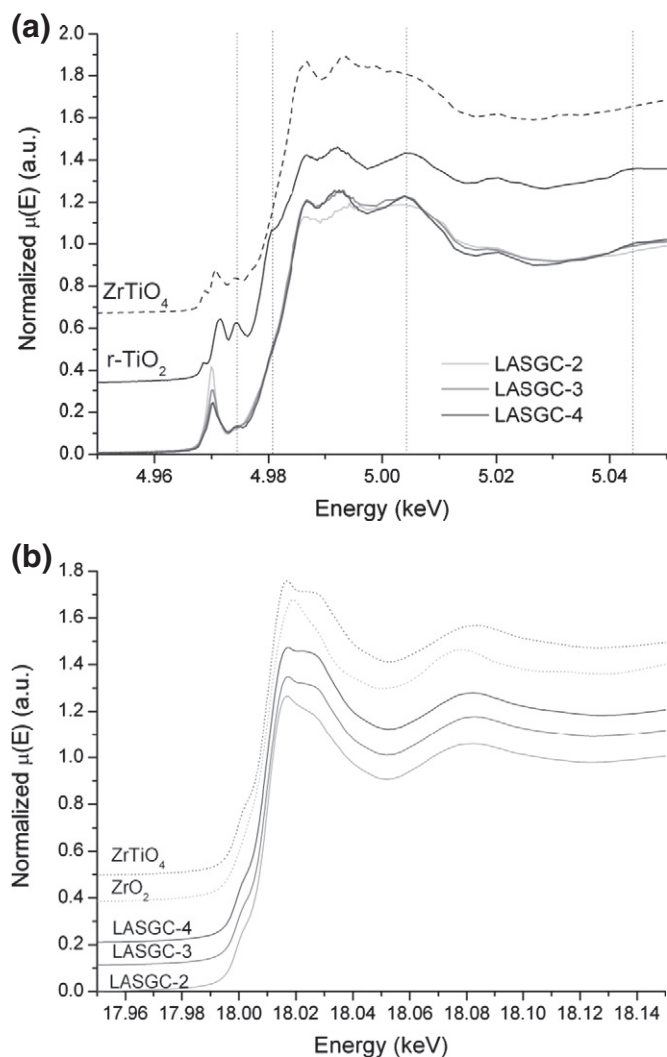


**Fig. 12.** XANES spectra of (a) LASGC-2, LASGC-3, LASGC-4, ZrTiO<sub>4</sub> and TiO<sub>2</sub> (rutile) at Ti K-edge; b) LASGC-2, LASGC-3, LASGC-4 and ZrTiO<sub>4</sub> samples and ZrO<sub>2</sub> (baddeleyite) at Zr K-edge.

conditions of crystallization during heat-treatment in LAS glasses are out of equilibrium. Therefore, it is possible that Zr<sub>1-x</sub>Ti<sub>1+x</sub>O<sub>4</sub> phases highly enriched in Ti ( $x > 0.34$ ) occur in the LASGC-3 and 4 samples. These phases could have medium-range order similar to that of r-TiO<sub>2</sub>, because the arrangements of the Ti-/Zr-octahedra are close in both phases (corner-linked chains of edge-linked octahedra in both cases).

XANES spectra of LASGC-*x* glass-ceramics at Zr K-edge give similar results. The Zr environment changes after heat-treatment due to the formation of ZrTiO<sub>4</sub>. LASGC-3 and LASGC-4 Zr-K edge XANES spectra closely match the ZrTiO<sub>4</sub> XANES spectrum (Fig. 12b), indicating that nearly all the Zr<sup>4+</sup> cations are in a ZrTiO<sub>4</sub>-type environment in these glass-ceramics (i.e. no Zr<sup>4+</sup> cations would be present in the residual glass). By comparison, the Zr environment in the LASGC-2 glass-ceramic is closer to the spectrum of Zr in 7-fold coordination as in ZrO<sub>2</sub> (baddeleyite), this phenomenon being not well explained.

#### 4. Discussion

From the optical transmission, diffuse reflectance and EPR results, it appears that the LAS-*x* glasses' yellowish color is mainly due to Ti<sup>4+</sup>-O<sup>2-</sup> charge transfer bands and not to Ti<sup>3+</sup> d-d absorption. Ti<sup>4+</sup> cations are in a mixture of fourfold and fivefold coordination states according to the Ti K-edge XANES spectra, in these LAS glasses.

Two charge transfer bands at 4.9 eV and 6.1 eV are observed in the diffuse reflectance optical spectra that are due to the splitting of the Ti d level in this four- and fivefold coordination state distributions. This average Ti environment is maintained up to 4 mol% TiO<sub>2</sub>, within the detection limit of the XANES spectra. However, the appearance of a CT band at 4.4 eV in the optical spectra when the TiO<sub>2</sub> concentration reaches 3 and 4 mol%, indicates that some modification of the Ti environment occurs and is deleterious to the absorption in the near UV range.

The association of the transmission and reflectance spectra clearly indicates that the origin of the browner coloration of the LASGC-*x* glass-ceramics lies in both the Rayleigh light scattering by nano-crystals in the 400–600 nm visible range and in the gap absorption of Zr<sub>1-x</sub>Ti<sub>1+x</sub>O<sub>4</sub> crystals in the 200–400 nm near-UV range. The shift detected in the near UV-visible range of the spectra (350–400 nm) of the LASGC-*x* glass-ceramics with increasing TiO<sub>2</sub> concentration from 2 to 4 mol% can be explained by the formation of Zr<sub>1-x</sub>Ti<sub>1+x</sub>O<sub>4</sub> and TiO<sub>2</sub> (rutile) crystals and/or Zr-doped TiO<sub>2</sub> crystals (with a structure close to ZrTiO<sub>4</sub>). Indeed, the onset of the optical gap of the LASGC-4 sample corresponds to that of TiO<sub>2</sub>.

Moreover, the formation of the Ti-enriched Zr<sub>1-x</sub>Ti<sub>1+x</sub>O<sub>4</sub> phase corresponds to the broad crystallization peak before the β-quartz crystallization on DTA curves of LAS-3 and LAS-4 glasses (Fig. 2). The corresponding XRD pattern presents only one broad diffraction peak at 30.5°, so that the precise determination of this phase is difficult. Notably, Zr<sub>1-x</sub>Ti<sub>1+x</sub>O<sub>4</sub> phases ( $x = 0$  and  $x = 0.34$ ) present major diffraction peaks in this 2 theta range but rutile does not.

Ti K-edge XANES spectra as well as TEM observations give us clues about the formation of this Ti enriched Zr<sub>1-x</sub>Ti<sub>1+x</sub>O<sub>4</sub> phase. The Ti-K edge spectra of LASGC-3 and LASGC-4 clearly contain edge-crest feature characteristic of the TiO<sub>2</sub> rutile phase with only minor contribution of Ti<sup>4+</sup> ions in the other phases (the residual glassy phase and possibly the β-quartz phase, approximately 19% for LASGC-4). Moreover, as ZrO<sub>2</sub> is the limiting oxide for Zr<sub>1-x</sub>Ti<sub>1+x</sub>O<sub>4</sub> crystallization and as its content was kept constant in all glasses (1 mol%, Table 1), only the occurrence of a Ti-enriched Zr<sub>1-x</sub>Ti<sub>1+x</sub>O<sub>4</sub> phase incorporating most of the Ti<sup>4+</sup> ions can account for the major contribution of <sup>16</sup>Ti species inferred from the spectra. At last, the TEM images of the LASGC-3 and LASGC-4 samples put in evidence an increasing amount of droplet-shape Zr- and Ti-bearing crystals attributed to this Zr<sub>1-x</sub>Ti<sub>1+x</sub>O<sub>4</sub> phase.

#### 5. Conclusion

The origin of the color of LAS glasses and glass-ceramics was studied by varying the TiO<sub>2</sub> concentration. It was shown that the glass color is due to Ti<sup>4+</sup>-O<sup>2-</sup> charge transfer band and not to Ti<sup>3+</sup>. When the glass is heat-treated, various phenomena occur and the color darkens. Using comparison of transmission spectra and diffuse reflectance spectra, the transmission decrease in the blue range (400–600 nm) can be assigned to the Rayleigh light scattering by the nano-crystals. Furthermore, the shift of the near-UV absorption towards the visible range (350–400 nm) could be linked to the gap absorption of Zr<sub>1-x</sub>Ti<sub>1+x</sub>O<sub>4</sub> solid solution whose Ti content increases with the TiO<sub>2</sub> concentration and exceeds the *x* value reported for the Zr<sub>1-x</sub>Ti<sub>1+x</sub>O<sub>4</sub> thermodynamic domain.

#### Acknowledgments

This work was supported by Saint-Gobain Recherche (Aubervilliers, France) and the Eurokera Company (Château-Thierry, France). XANES data were collected on the beamline 20-BM at the Advanced Photon Source (APS), Argonne National Laboratory (IL, USA). Use of the Advanced Photon Source was supported by the U. S. Department of Energy, Office of Science, Office of Basic Energy Sciences, under contract no. DE-AC02-06CH11357. The authors would like to thank particularly C. Sun from the APS beamline 20-BM for his availability and assistance during XANES measurements. J.-M. Guigner from IMPMC (Paris, France)

is acknowledged for TEM measurements. Moreover, the authors would also like to thank L. Cormier from IMPMC (Paris, France) for providing several reference compounds for XANES measurements.

## References

- [1] W. Höland, G. Beall, *Glass–Ceramic Technology*, The American Ceramic Society, Westerville OH, 2002.
- [2] H. Bach, *Low Thermal Expansion Glass–Ceramics*, Springer, Berlin, 1995.
- [3] G. Beall, L. Pinckney, *J. Am. Ceram. Soc.* 82 (1999) 5.
- [4] S. Bhattacharyya, T. Höche, J.R. Jinschek, I. Avramov, R. Wurth, M. Müller, C. Rüssel, *Cryst. Growth Des.* 10 (2010) 379.
- [5] T. Höche, M. Mäder, S. Bhattacharyya, G.S. Henderson, T. Gemming, R. Wurth, C. Rüssel, *I. Avramov, CrystEngComm* 13 (2011) 2550.
- [6] T. Höche, C. Patzig, T. Gemming, R. Wurth, C. Rüssel, I. Avramov, *Cryst. Growth Des.* 12 (2012) 1556.
- [7] M. Guedes, A.C. Ferro, J.M.F. Ferreira, *J. Eur. Ceram. Soc.* 21 (2001) 1187.
- [8] Q. Sun, J. Shi, *J. Phys. Chem. C* 114 (2010) 3230.
- [9] C.R. Bamford, *Colour Generation and Control in Glass*, Elsevier Scientific Publishing Co., Amsterdam and New York, 1977.
- [10] N.A. El-Shafi, M.M. Morsi, *J. Mater. Sci.* 32 (1997) 5185.
- [11] P.A. Bingham, J.M. Parker, T.M. Searle, I. Smith, *J. Non-Cryst. Solids* 353 (2007) 2479.
- [12] L.B. Glebov, E.N. Boulos, *J. Non-Cryst. Solids* 242 (1998) 49.
- [13] R.G. Burns, *Ann. Rev. Earth Planet. Sci.* 9 (1981) 345.
- [14] T.I. Chuvaeva, E.V. Podushko, *Opt. Mekh. Prom.* 43 (1976) 40.
- [15] F. Farges, C. Ponader, G.E. Brown, *Geochim. Cosmochim. Acta* 55 (1991) 1563.
- [16] C. Romano, E. Paris, B.T. Poe, G. Giuli, D.B. Dingwell, A. Mottana, *Am. Mineral.* 85 (2000) 108.
- [17] S. Baghshahi, M.P. Brungs, C.C. Sorrell, H.S. Kim, *J. Non-Cryst. Solids* 290 (2001) 208.
- [18] P. Loiseau, D. Caurant, O. Majérus, N. Baffier, C. Fillet, *J. Mater. Sci.* 38 (2003) 853.
- [19] A. Ramos, M. Gandais, J. Petiau, *J. Phys. C8* (1985) 491.
- [20] K. Morinaga, H. Yoshida, H. Takebe, *J. Am. Ceram. Soc.* 77 (1994) 3113.
- [21] A. Elvers, R. Weißmann, *Glastech. Ber. Glass Sci. Technol.* 74 (2001) 32.
- [22] E.S. Dunaeva, I.A. Uspenskaya, K.V. Pokholok, V.V. Minin, N.N. Efimov, E.A. Ugolkova, E. Brunet, *J. Non-Cryst. Solids* 358 (2012) 3089.
- [23] H.D. Schreiber, G.B. Balazs, *J. Non-Cryst. Solids* 71 (1985) 59.
- [24] R. Brückner, *J. Non-Cryst. Solids* 71 (1985) 49.
- [25] F. Farges, G.E. Brown, J.J. Rehr, *Phys. Rev. B* 56 (1997) 1809.
- [26] A.E. McHale, R.S. Roth, *J. Am. Ceram. Soc.* 66 (1983) C18.
- [27] *Colorimetry: Understanding the CIE System*, in: J. Schanda (Ed.), John Wiley & Sons, Hoboken, New Jersey, 2007.